Review

Plasmonics in Photonic Integrated Circuits

Giovanni Magno *, Vy Yam , Béatrice Dagens *

Posted Date: 17 October 2023

doi: 10.20944/preprints202310.1041.v1

Keywords: plasmonics; photonic integrated circuits; surface plasmon; nanotweezers; couplers; strong coupling; magnetoplasmonics; nanoantennas

Review

Plasmonics in Photonic Integrated Circuits

Giovanni Magno [1,*], Vy Yam [2] and Béatrice Dagens [2,*]

[1] Department of Electrical and Information Engineering (DEI), Polytechnic University of Bari, Bari, Italy
[2] Université Paris-Saclay, CNRS, Centre de Nanosciences et de Nanotechnologies, Palaiseau, France
* Correspondence: giovanni.magno@poliba.it (G.M.); beatrice.dagens@universite-paris-saclay.fr (B.D.)

Abstract: The development of integrated, compact, and multifunctional photonic circuits is crucial to increase the capacity of all-optical signal processing for communications, data management or microsystems. Plasmonics brings compactness to numerous photonic functions, but its integration into circuits in not straightforward due to insertion losses and poor modes matching. The purpose of this article is to detail the integration strategies of plasmonic structures on dielectric waveguides, and to show through some examples the variety and the application prospect of integrated plasmonic functions.

Keywords: plasmonics; photonic integrated circuits; surface plasmon; nanotweezers; couplers; strong coupling; magnetoplasmonics; nanoantennas;

1. Introduction

The use of optical signals for the implementation of complex computing, information processing or communication networks is nowadays essential to meet the growing demand for data exchange. The possibility of parallelizing optical carriers thanks to spectral multiplexing or to specific information encodings are among the key features of the all-optical solution. Photonic integrated circuits (PICs) [1–3] have been developed to generate complete optical systems and to simplify the use of different optical functions from source to modulation and signal detection. By using manufacturing techniques inspired by microelectronics, planar waveguide circuits have made it possible to achieve two complementary objectives: (1) to control the propagation of the optical signal in a 2D system with very low losses; (2) to facilitate the serial or parallel association of several functions without the use of spatial optical elements. Guided planar optics thus enables to integrate in a compact way optical elements whose lateral dimension is of the order of the wavelength in the material. But this dimension remains diffraction limited and cannot be further reduced.

Plasmonics has been a strongly studied field since the 2000s for its unique ability to concentrate light on a sub-wavelength scale. This involves confining light in the form of surface plasmon-polaritons (SPPs): these resonant quasiparticles result from the strong coupling between an electromagnetic wave and an electrical polarization wave carried by the surface conduction electrons of certain metals. Copper, gold, silver, and aluminum exhibit plasmonic responses from near-infrared (IR) to near-ultraviolet (UV) in ascending order of resonance frequencies. The electromagnetic wave that is "hooked" to the surface of the metal by plasmonic interaction has an evanescent wave profile on either side of the interface and contains a very high optical power density. Light is slowed down and concentrated at the subwavelength scale on the surface of the metal, available for exalted interactions with any entity or material on or near the surface. Plasmons can be either "propagative" on the surface of a metal film, or "localized" in metal nanostructures . Several properties result from their specific spatial profile and resonance: the miniaturization of optical functions, the enhancement of non-linear optical interactions, a strong spectral and polarization dependence and therefore a high sensitivity of their resonance to the near environment. Finally, the technological manufacture of plasmonic films or structures is compatible with low-cost processes, in a reduced number of steps and with good tolerance.

Preprints (www.preprints.org) | NOT PEER-REVIEWED | Posted: 17 October 2023 doi:10.20944/preprints202310.1041.v1

However, there are two types of constraints to the use of plasmons in optical functions: (1) the high optical losses induced by the interaction of the wave with the metal allow the use of plasmons only sparingly; (2) the plasmons excitation from electromagnetic waves requires complex strategies, due to their propagation constants which are intrinsically higher, or even much higher, than those of electromagnetic waves in the surrounding environment. These two limitations can be simultaneously addressed by the combined use of photonic circuits and plasmonic structures. In this case, the integration of plasmonic structures on photonic circuits [7], or more elementarily on waveguides, allows benefiting from the advantages of both components (low losses of dielectric waveguides and compactness of plasmons). Nevertheless, this implies properly interfacing with each other, which is made difficult by the very different spatial extension of dielectric and plasmonic modes, which comes along with the very different modules of propagation constants.

In this context, the purpose of this article is on the one hand to review the strategies for integrating (localized or propagative) plasmonic structures on dielectric waveguides, and on the other hand to show by some examples the diversity and application potential where the synergic plasmonic functions integration could make a breakthrough.

2. Integration and excitation of plasmonic structures

The utilization of plasmonics within photonic circuits poses a significant challenge due to the contrasting spatial characteristics of plasmonic and dielectric modes. The primary hurdle lies in achieving optimal optical integration, and an impedance adaptation, between metallic structures and dielectric waveguides. This integration typically involves a mode coupling region, the length of which depends on the specific interfacing mechanism. To assess the quality of the interfacing, the relevant indicator is the coupling efficiency, which is defined by the ratio between the power available in the waveguide at the exit of the transfer zone and that in the dielectric guide before the transfer zone. By this definition, coupling efficiency therefore includes losses of all kinds (ohmic, related to the mismatch of modes...) generated in the coupling region. In this section, we will delve into these interfacing challenges for both propagative and localized plasmon families.

2.1. Propagative surface plasmon

Propagative surface plasmon is generated at the interface between a metal and a dielectric material. It can propagate at several wavelengths distance along this interface. It has the characteristic profile of transverse magnetic (TM) wave, featuring its primary electric field component perpendicular to the interface and a secondary, smaller component in the propagation direction. Its profile also exhibits an exponential decrease, forming an evanescent profile on each interface side, as shown in Figure 1a,b.

Propagative SPP is analytically described by its dispersion curve, which is established by solving the Maxwell equations in the case of the double exponential profile [5]:

$$k_{sp}(\omega) = \frac{\omega}{c}\sqrt{\frac{\varepsilon_{ext}.\varepsilon_m}{\varepsilon_{ext}+\varepsilon_m}} \quad (1)$$

where k_{sp} is the wavevector of the SPP, and ε_{ext} and ε_m are the permittivity of the dielectric and the metal materials, respectively. The profile of the dispersion curve is represented in Figure 2 in the case of air-gold and InP-gold plasmonic modes, where gold permittivity spectrum is approximated by Drude model [8,9]. ω_p is the plasma resonance pulsation in the metal. These curves reveal the main properties of SPPs: (1) the SPP dispersion curve never crosses the light line of the surrounding dielectric medium, and remains below it, i.e., SPPs propagate with higher propagation vector (or higher effective index) than the electromagnetic wave in this medium; (2) when SPP frequency approaches the plasmonic resonance, i.e., $\omega_{sp}/2\pi$, the dispersion curve becomes horizontal: the SPP propagates very slowly (group velocity is near zero) and is very confined (high k); (3) the plasmonic resonance frequency strongly depends on the surrounding medium index.

Preprints (www.preprints.org) | NOT PEER-REVIEWED | Posted: 17 October 2023 doi:10.20944/preprints202310.1041.v1

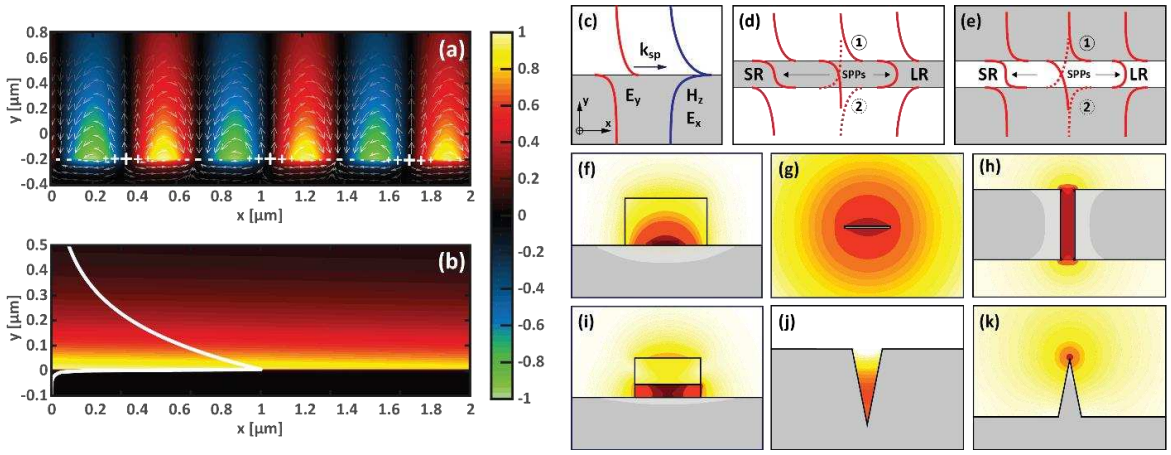

Figure 1. (**a**,**b**) Profile of a surface plasmon polariton (SPP) on an air-Au interface: (**a**) The color scale corresponds to the normalized real part of the x-component of the electric field. More specifically, the white arrows indicate the orientation of the total E field, while the + and – markers indicate the distribution of free charges on the Au surface. (**b**) The color gradient indicates the total electric field intensity. The superposed white line depicts the distribution of the intensity of the electric field x-component. (**c**–**k**) Plasmonic modes calculated for different waveguide geometries: (**c**–**e**) Real part (red) of the electric field y-component when the propagation occurs along the x-direction (in-plane with respect to the figure plane); the label LR (SR) indicates the symmetric (asymmetric) coupling of two surface plasmons (SPPs) generating a "long-range" ("short-range") mode. (**f**–**k**) electric field intensity of the wave in the case of propagation occurs along the z-direction (out-of-plane with respect to the figure plane). Structures inspired by [10].

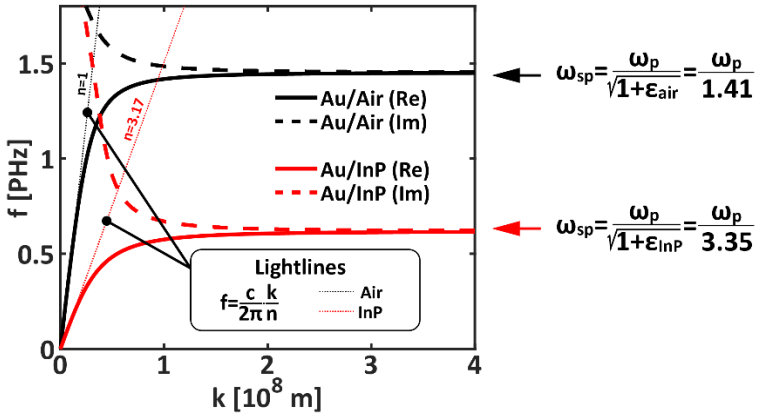

Figure 2. Dispersion curves of propagative surface plasmons at the gold-air interface and gold-InP interface. The solid (dashed) lines represent the contribution solely from the real (imaginary) part of the complex permittivity.

Several types of propagative plasmonic waveguides have been proposed, as schematized in Figure 1c–k. Some of them are designed to allow long range propagation (LR), minimizing the direct interaction between the wave energy and the metal thanks to coupled SPPs on each side of a metallic thin film (Figure 1d,g), or in a metallic slot waveguide (Figure 1e,h–j). The LR-SPP is the symmetric (phase) supermode resulting from SPP modes coupling and is always associated to the asymmetric one, the SR (short range) SPP which is more lossy [10].

To benefit of their high confinement and compactness while limiting the induced losses, such plasmonic waveguides can be selectively integrated into conventional single-mode dielectric photonic waveguides. The typical interfacing schemes (Figure 3) exploit either progressive transition (evanescent coupling, grating coupling) or butt-joint transition between the photonic and the plasmonic

Preprints (www.preprints.org) | NOT PEER-REVIEWED | Posted: 17 October 2023 doi:10.20944/preprints202310.1041.v1

waveguides. Butt-joint transition offers poor performance because of the high mode shape mismatch between the plasmonic and the photonic modes (Figure 3a top) and will not be addressed here.

The underlying physical mechanism harnessed through evanescent coupling (depicted in Figure 3b) or grating coupling (Figure 3c) can be described by examining the dispersion curves of the involved modes (shown in Figure 3d,e): the dispersion curve of the SPP at the interface between a metal and a dielectric material (represented by the red curve) is situated significantly below the light line of the corresponding dielectric (characterized by an index n_{ext}), for modes with the strongest plasmonic character, particularly when the SPP dispersion curve becomes horizontal. The plasmon cannot be excited by an electromagnetic wave with a propagation constant lower than k_{sp}. In the integrated configuration where the plasmonic waveguide (comprising a metallic film) is positioned on a multilayer dielectric waveguide (as depicted in Figure 3b), the dielectric waveguide mode effective index n_d is higher than the surrounding dielectric material index, by construction ($n_d>n_{ext}$): this property can be directly used to excite the SPP when $k_d \cong k_{sp}$, since both dispersion curves cross each other (see the dispersion diagram in Figure 3d). If the polarization of the dielectric guided mode can provide the electric field z- and x- components required for the SPP excitation, modes coupling occurs and generates two photonic-plasmonic hybrid modes (or supermodes), with respectively symmetric and antisymmetric field profiles, and indices n_p et n_i (Figure 3a, middle). The half-beating length of these supermodes determines the coupling length of both waveguide modes, which is related to their wavevector difference:

$$Lc = \left| \frac{1}{2} \frac{\lambda}{n_i - n_p} \right|. \quad (2)$$

After a propagation distance of L_c through the coupling region, the energy of the dielectric guided mode is totally transferred into the SPP. Such mode coupling is called "evanescent coupling" because it involves the evanescent tails of the guided modes. The required condition ($n_d>n_{ext}$) is more easily realized when the targeted SPP is on the (thin enough) metallic film opposite side with respect to the dielectric waveguide, as shown in Figure 3b: indeed, the outside material can have a low refractive index, independent of the guided mode effective index. On the dispersion curves map, this interaction induces anticrossing of both curves. In case of high contrast between n_{ext} and n_d, the involved plasmonic mode dispersion curve is almost flat (horizontal), and thus the generated supermodes have very different effective indices: the higher is the supermode indices difference, the shorter is the coupling length. Thus, such mechanism is particularly efficient when the contrast between n_{ext} and n_d is high. Delacour *et al.* [11] have realized this for example in the case of an SOI waveguide and a Cu plasmonic slot waveguide at 1.55µm. The experimental coupling length equals 0.9µm and the coupling efficiency is estimated at 70%. In another example involving polymer waveguides, Magno *et al.* [12] demonstrated numerically the coupling between a SU8 on glass waveguide and a buried plasmonic waveguide at 633 nm, with L_c=5.3µm and a coupling efficiency of 88%. The use of SOI waveguides is particularly interesting since in that case the dielectric waveguide mode has a high effective index. However, when coupling the fundamental TM mode of a high-contrast dielectric waveguide (with a high effective refractive index) to the LR-SPP mode of a thin-film plasmonic waveguide embedded in a low refractive index medium (with a low effective refractive index), it can be beneficial to employ layers of dielectric material with higher refractive indices that encapsulate the plasmonic waveguide. This helps satisfy the phase-matching condition as shown in [13].

If the condition $k_d \cong k_{sp}$ cannot be fulfilled, the guided dielectric mode must interact with a complementary structure (Figure 3c,e) to increase its wavevector module up to k_{sp} ($k_{sp}=k_d+\delta k$): the interaction of the dielectric waveguide mode with a periodic grating (period Λ) serves this purpose since it generates spatial harmonics whose constant propagations equal $k=k_d+p\,2\pi/\Lambda$, where p is a relative integer. The first harmonic (p=1) is the most intense: by choosing Λ so that $k_{sp}-k_d=2\pi/\Lambda$ the grating provides the dielectric waveguide mode with the missing component δk to excite the SPP at the dielectric/metal interface (each surface of the metal can be targeted, by proper choice of δk). In the case of strong mismatch of the dielectric and plasmonic waveguides (i.e., if the targeted mode has a strong plasmonic character, with very high k_{sp}), successive gratings with decreasing period can be

Preprints (www.preprints.org) | NOT PEER-REVIEWED | Posted: 17 October 2023 doi:10.20944/preprints202310.1041.v1

used for a progressive adaptation, with the risk of long and lossy transition. Tetienne et al. [14] have shown an integrated coupler made of a metallic grating for the transition between a semiconductor waveguide and a plasmonic gold film at 1.3µm: the mode transfers along a 5.5µm transition, with a global excitation efficiency of 24%.

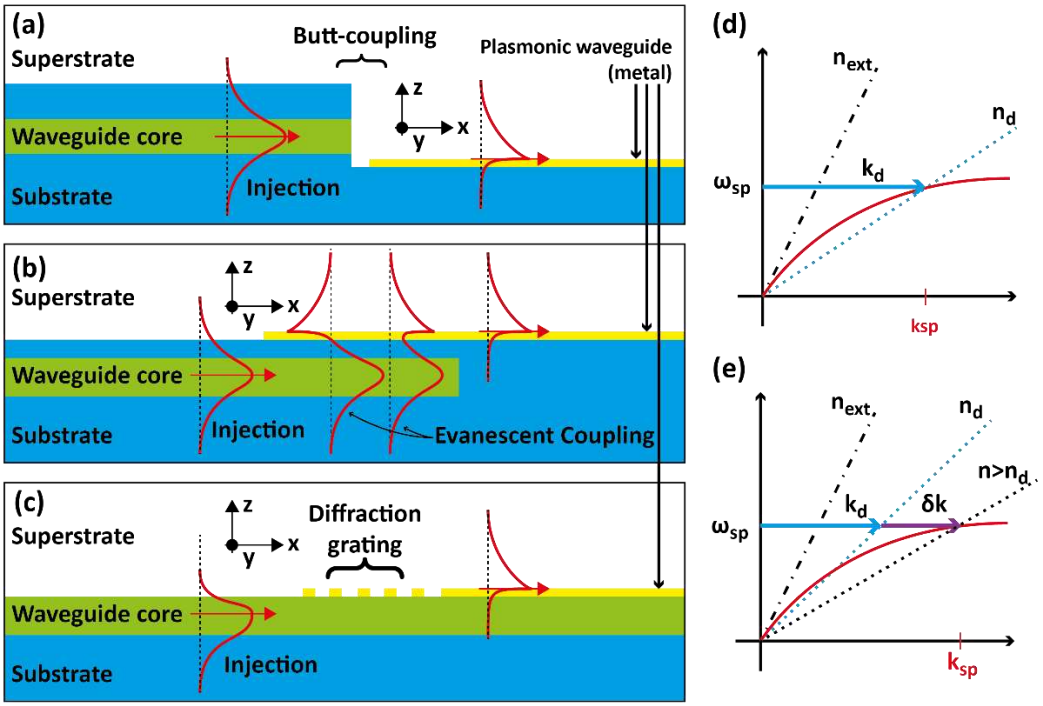

Figure 3. (**a**–**c**) Diagram illustrating three different typical ways of coupling a dielectric waveguide with a plasmonic waveguide: (**a**) end-fire coupling, (**b**) evanescent coupling, and (**c**) coupling via a diffraction grating. (**d**) The wave vector k_d of the guided mode in the dielectric waveguide is equal to that required to excite the plasmonic mode, k_{sp}. (**e**) The wave vector of the dielectric waveguide mode is not sufficient and requires an additional contribution δk, arising from the diffraction grating, to match that of the plasmonic waveguide mode.

2.2. Localized surface plasmon

Localized surface plasmons (LSP) result from the plasmonic excitation in low-dimensional metallic structure with typical dimensions lower than the wavelength in the metal. LSP modes are eigenmodes of such a subwavelength metallic structure which behaves as a dipole or a multipole. The LSP dipolar response of the nanostructure to the electromagnetic excitation is characterized by its polarizability, which has an analytical expression in case of 'simple' shapes and homogeneous surrounding medium [15].

The excited dipole in a plasmonic nanoparticle radiates itself an electromagnetic wave of the same frequency, which can excite another plasmonic nanostructure with similar resonance: such a way, plasmonic nanostructures assembly may support collective resonances, and/or propagate energy from one to the next. LSP chain dispersion curve can be thus established, by using analytical model in a homogeneous medium [16], or by numerical methods in the general case. For instance, in Figure 4 is reported the dispersion curve of a plasmonic chain constituted of gold nanocylinders with elliptical cross-section placed on top of a semi-infinite Si substrate, calculated by means of the FDTD method. The LSP chain dispersion curve displays a similar overall behavior as the SPP: it is positioned below the light line and exhibits a nearly horizontal slope at the highest k vectors. In other words, the collective modes of the LSP chain propagate through the chain elements as in a waveguide, despite the intrinsic discontinuity of the metallic elements.

Preprints (www.preprints.org) | NOT PEER-REVIEWED | Posted: 17 October 2023 doi:10.20944/preprints202310.1041.v1

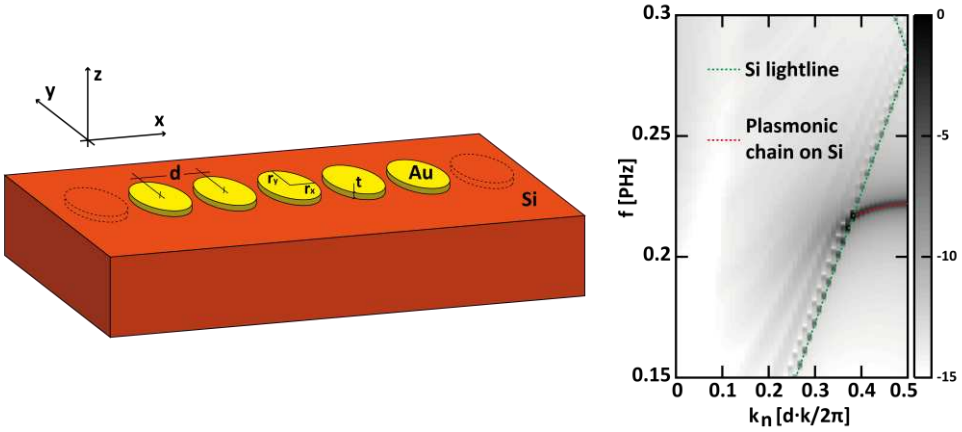

Figure 4. (**left**) Sketch of an infinite plasmonic chain of gold ellipsoidal nanocylinders placed on top of a semi-infinite Si substrate. (**right**) FDTD calculated dispersion curve of the plasmonic transverse chain mode when d = 150 nm, r_x = 42.5 nm, r_y = 100 nm, and t = 30 nm. The red and the green dashed curves highlights the plasmonic chain mode and the Si lightline, respectively.

Furthermore, chains of plasmonic nanoantennas have the ability to support topologically non-trivial modes (edge states resembling topological insulators) [17–21], bound states in the continuum [22–24] and surface lattice resonances [25–28].

LSP in a subwavelength structure enables very high light confinement, with enhanced miniaturization and electromagnetic field concentration with respect to 2D plasmonic films. Nevertheless, the excitation of a single LSP structure is very inefficient because of the high mismatch between its resonant mode size and diffraction limited electromagnetic waves. The excitation efficiency of such a single nanostructure deposited on a silicon nitride waveguide reaches less than 10% (9.7% in [29]). To transfer all the energy of the dielectric guided mode into an LSP, a viable solution is to exploit the waveguides evanescent coupling as shown above, considering a plasmonic chain instead of the plasmonic metallic film [30]. The typical structure is made of a MNP metallic nanoparticles (MNPs) chain integrated on or near a dielectric waveguide (Figure 5). The chain can be designed to propagate either TE or TM modes and can be in any position near the waveguide if their relative distance allows the evanescent tail of the dielectric mode to overlap with the LSPs. In addition to enabling the LSP excitation, such strongly coupled structure has specific properties, as described below:

Coupling efficiency:

Figure 5 shows FDTD calculations of a TE mode in a dielectric waveguide evanescently coupled to a LSP chain. The (infinite) LSP chain is directly deposited on a SOI waveguide, and Figure 5b–d reveals the anticrossing of both dispersion curves which generates the resulting odd and even supermodes. The strong coupling between both waveguides, in addition to the low slope of the LSP chain curve induces supermodes with very different indices and thus a very short coupling length. Depending on the wavelength, the fundamental TE mode of a SOI waveguide can be totally transferred in the 4th or 5th MNP of the finite chain [30], which corresponds to a ~600 nm coupling length (Figure 5f). The coupling efficiency is near 99% in the case of a 5 MNP chain (Figure 5e). Due to a lower dielectric effective index, the optimal configuration in the case of a Si_3N_4 waveguide at 633 nm enables a total transfer of the mode energy in an 8 MNP chain with a coupling length ~800 nm.

In fact, the energy transfer efficiency is improved with respect to a single MNP case as soon as a second MNP is involved ('dimer' chain). In return, however, the chain length increase implies ohmic losses increase. In order to exploit the high electromagnetic power density at the surface of a nanoparticle, the best compromise must be thus identified between the efficient energy transfer induced by the collective resonance in the chain and the ohmic losses limitation.

Preprints (www.preprints.org) | NOT PEER-REVIEWED | Posted: 17 October 2023 doi:10.20944/preprints202310.1041.v1

Strong coupling:

In the configuration presented in Figure 5a, the strong coupling [31] between the plasmonic and SOI waveguides induces additional distinctive characteristics specific to this system. Firstly, over a wide range of frequencies, the supermodes propagate in a vortex-like manner. These vortices are related to slow modes [32] and can be also characterized by their phase profile along the chain [33]. Secondly, due to strong coupling, supermodes can be excited also beyond the light lines of the different materials surrounding the plasmonic chain. This entails that they can be excited as radiative modes above the light line of the confinement layer (silica here), and/or below the highest index material light line (silicon here), in the non-guided mode region (see the dispersion diagrams in Figure 5b,c). In consequence the plasmonic mode hybridization can modify their radiative or guided nature, or even extend their possible frequency range.

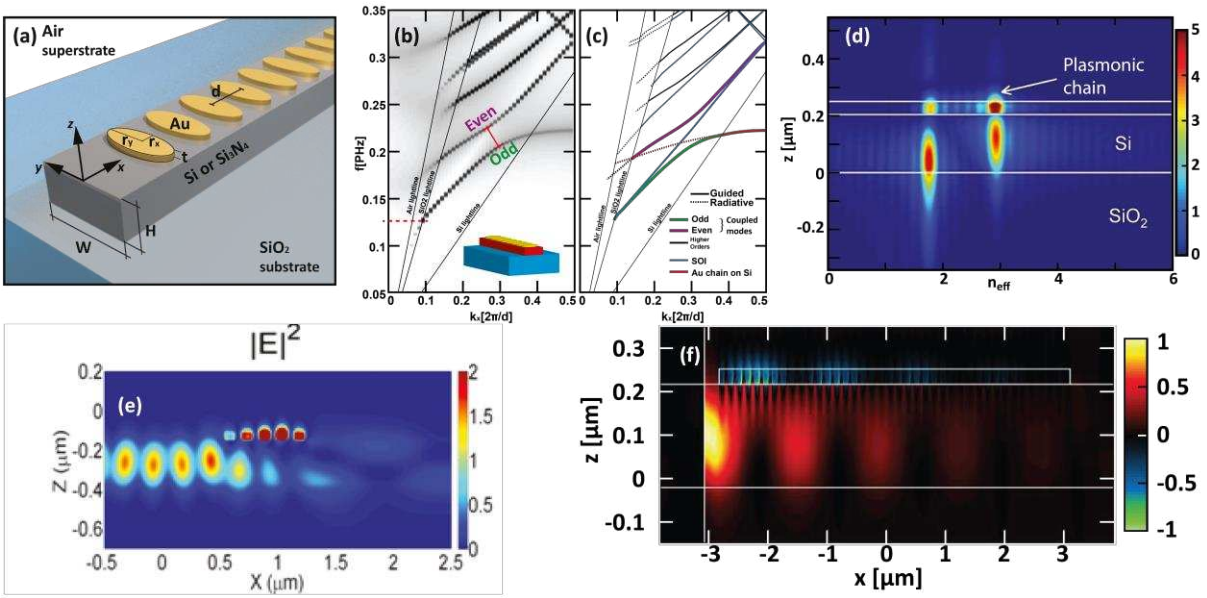

Figure 5. Localised plasmon waveguide integrated on SOI (TE mode) (**a**) Sketch of the structure. (**b**,**c**) FDTD calculated dispersion curves for d = 150 nm, r_x = 42.5 nm, r_y = 100 nm, t = 30 nm (the permittivity of gold is obtained using a Drude model fitted to ellipsometric measurements). (**d**) A typical spatial distribution of the two supermodes. (**e**,**f**) Electric field intensity in the case of a finite chain of (**e**) 5 or (**f**) 20 nanoparticles. Inspired by [32].

Moreover, nanoantenna arrays integrated on waveguides can take advantage of tapering their dimensions within the integration plane to achieve enhanced control over coupling characteristics. For instance, tapering the period of the plasmonic array enables efficient mode conversion and excitation of higher-order modes in the waveguide [34].

3. Surface plasmons in photonic integrated circuits

Surface plasmons in PICs are expected to considerably improve some photonic functions thanks to the subwavelength light concentration and the local field enhancement they induce. Reciprocally the use of guided photonics to excite plasmonic structures leads to very efficient light coupling in these structures. Improvement is particularly marked in the case of very compact localized plasmonic patterns. We will focus here on four examples of different uses of integrated plasmonics.

3.1. LSPR for molecules biosensing

Plasmonic biosensing [35–39] was firstly mainly based on functionalized gold films and propagative plasmons (SPR technology), before to exploit localized surface plasmons in metallic nanostructures arrays on glass (LSPR technology) [40,41], as in present commercialized setups. Such

Preprints (www.preprints.org) | NOT PEER-REVIEWED | Posted: 17 October 2023 doi:10.20944/preprints202310.1041.v1

functionalized substrates are used in 3D complex optics systems made of prisms and lenses with the following principle: metallic (gold) nanostructures are grafted with molecule receptors (often thiols), and molecules to be detected are brought to these receptors by microfluidic system. The trapping of the molecules is detected by the plasmonic resonance shift induced by the complex index modification near the metallic structure, where a diffraction limited laser beam in Kretchman configuration excites the plasmon [42]. In LSPR systems, the sensor sensitivity is limited by the optical power available for each functionalized nanostructure, because of poor mode matching as explained above. By using the same detection principle, excitation of LSPs can be realized in guided configurations, with two main advantages:

- the excitation electromagnetic energy can be fully transferred in the LSP, like in the case of a 5 MNP chain [43], leading to an improved sensitivity,
- parallel or series sensing areas can be implemented on the chip, with the same optical source: the global analysis capacity is considerably enhanced.

Figure 6 shows such a guided LSPR sensor including a chain or 5 MNPs, and the resonance spectral shift induced by grafted thiol molecules which forms an equivalent layer of thickness t=2nm and of index n=1+Δn. This shift Δλ has been numerically evaluated and experimentally checked as corresponding to the relation $\Delta\lambda(\text{nm}) \approx 27\,(t(\text{nm}) \times \Delta n)^{0.75}$. The expected sensitivity to environment of this sensor integrated on SOI can reach a value up to 270nm/RIU (Refractive Index Unit) [43].

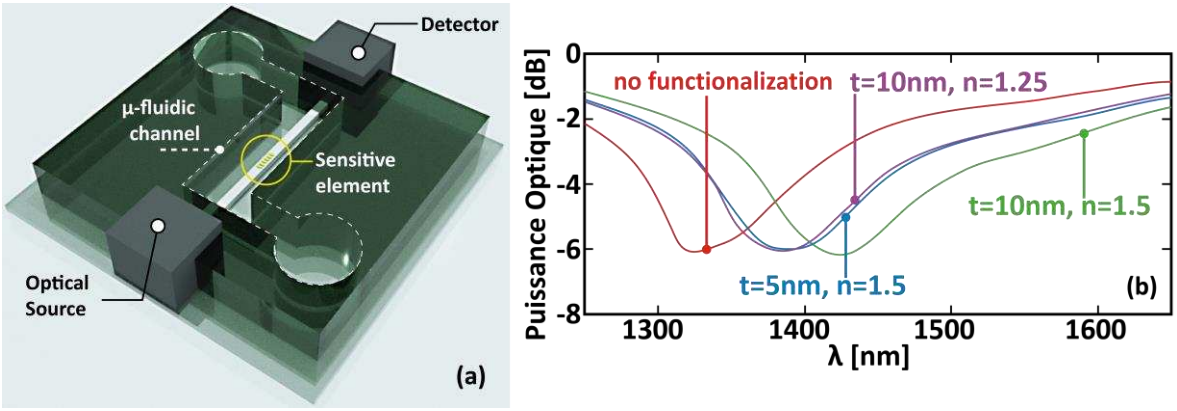

Figure 6. (**a**) Sketch of a sensor exploiting LSPRs: a chain of gold nanocylinders is integrated on top of a SOI waveguide within a microfluidic circuit. (**b**) Transmittance calculated for different equivalent thicknesses t of molecules grafted onto the metal pads [43]. Specifically, t represents the thickness of a layer having an index equal to n covering each NP. This result has been validated experimentally for t = 2 nm.

3.2. Plasmonic nano-tweezers and nano-manipulators

Tweezers and manipulators at nanoscale are in very high demand for biosensing and analysis of nano-objects. High electromagnetic density variation around plasmonic nanostructures enables optical tweezing based on the gradient force [44], which results from mechanical and optical momentum exchange between the object and the photons. Gradient force acts as an elastic trap for an object entering its influence area, with a stiffness proportional to the local optical power derivative.

Basis on optical tweezers

Optical tweezers are made of a focused optical beam, diffraction limited in the case of free space beam, which generates two forces on an object (Figure 7, left): the gradient force and the pressure (or diffusion or absorption) force. The former pulls the object towards the highest optical density, usually transversally to the optical beam and up to its center; the latter pushes the object along the beam propagation axis and direction. These forces are expressed as follows:

Preprints (www.preprints.org) | NOT PEER-REVIEWED | Posted: 17 October 2023 doi:10.20944/preprints202310.1041.v1

Gradient force: $\boldsymbol{F}_g = \frac{1}{4}\,\alpha_{Re}\nabla|\boldsymbol{E}|^2$

Pressure force: $\boldsymbol{F}_s = -\frac{1}{2}\,\alpha_{Im}\mathrm{Im}\{\boldsymbol{E}.\nabla(\boldsymbol{E}^*)\}$

where α is the object polarizability: $\alpha = \alpha_{Re} + j\alpha_{Im}$

The gradient force is thus the trapping force. It is proportional to the optical power density (or the electric field square modulus) gradient and to the object polarizability real part. The trapping strength is represented by its stiffness, defined by the exerted forces derivative. Negative (positive) stiffness corresponds to attractive (repulsive) force.

The trap characteristics can be evaluated as follows:

- If the trapped object doesn't modify the local electromagnetic field, the optical density map is calculated first, and then the trap characteristics are deduced from $\boldsymbol{F}_g$ et $\boldsymbol{F}_s$ calculation for different object positions.
- if the presence of the object induces a non-negligible perturbation, the optical field must be calculated, and the Maxwell stress tensor must be fully integrated for all the possible positions of the object.

Optimal trap, in terms of temporal and spatial stability, is obtained for object sizes slightly higher than the optical beam (or than the optical power density high variations area) to benefit from the highest gradients. Stable trapping criteria (from Ashkin [44]) state that the potential well must be higher than ten times the thermal energy $k_B T_0$. The total optical power can thus be used to increase the stability as well as the stiffness of a trap.

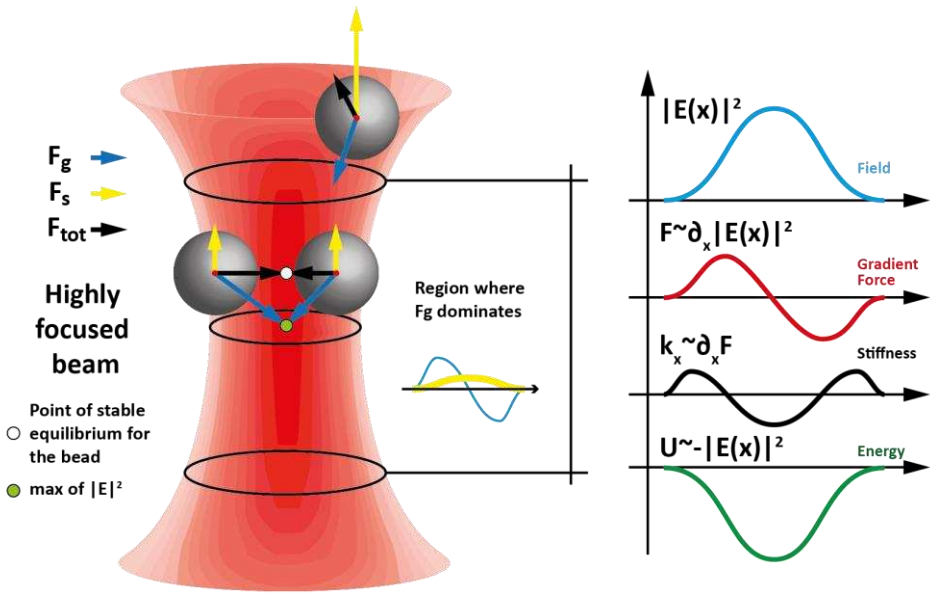

Figure 7. Sketch of optical tweezing in a gaussian beam. The total force $\mathbf{F}_{tot}$ represents the sum of the gradient force $\mathbf{F}_g$ and of the scattering force $\mathbf{F}_s$.

Optical beams enable the trapping of around 1 µm objects within a few mW power, compatible with biological objects whose index is around 1.3 (water). To trap smaller or less dense objects (for air or water quality analysis), more abrupt optical density gradients are required, such as those generated around plasmonic structures.

Plasmonic tweezers

Plasmonic (nano-)tweezers have been extensively studied, mainly in non-integrated configurations. Integrated localized plasmonics may enable extremely high gradient forces thanks to the powerful combination "high optical density" and "high excitation efficiency" of integrated resonant structures. Numerical and experimental demonstrations aim at trapping polystyrene beads of different diameters in the three published examples represented in Figure 8. In the first case (Figure

Preprints (www.preprints.org) | NOT PEER-REVIEWED | Posted: 17 October 2023 doi:10.20944/preprints202310.1041.v1

8a) the dimensions of metal nanostructures enable only propagative plasmons: the 5µm diameter disks are positioned along a 15µm grid on the top of a multimode waveguide; 1µm diameter PS beads are trapped with an injected power of 20 mW, leading to a trap stiffness of -17fN/µm. The second structure (Figure 8b) is designed for the trapping of 20 nm diameter beads, concentrating the light in the narrow gap of the butterfly structure: the theoretically achievable force reaches more than 650pN/W in the case of a 5nm gap. Comparable results are obtained by varying the dimer geometry within the integration plane, as illustrated in [45]. The third example corresponds to the integrated MNP chain which maximizes the LSP excitation: in the case of a 4 MNP chain, with a 150nm period, the exerted force on a 500nm diameter PS bead reaches ~40pN/W with a stiffness of -2408 fN/nm/W. The considered power refers to the power injected in the waveguide.

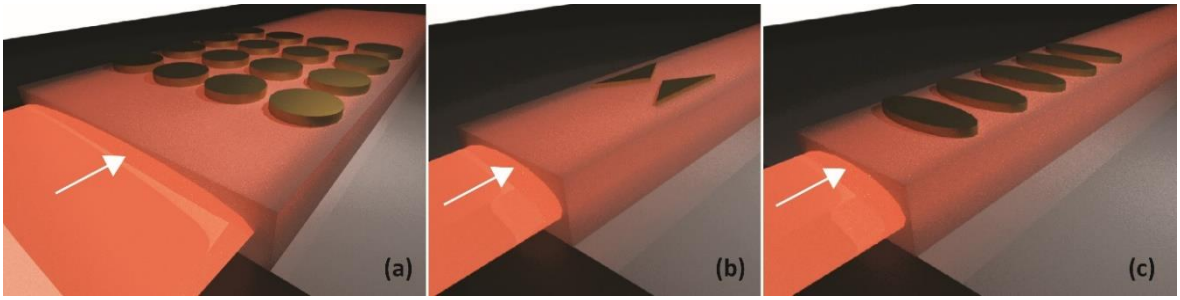

Figure 8. Plasmonic nanostructures integrated on top of a waveguide: (**a**) array of metallic pads supporting propagative resonances (SPP) (according to [46]); (**b**) single bowtie nanoantenna (according to [44]); (**c**) chain of coupled nanocylinders (according to [47]).

In this kind of chain, plasmonic modes generate high spot at the ellipsoidal nanocylinders edges, separated by around 200 nm (see Figure 9a). To trap nano-objects, the trap must be compact. The gap between MNP can be smaller to create a resonant nano-gap, like in the longitudinal dimer represented in Figure 9b. As simulated in Figure 9 (bottom, right), a gap lower than 40 nm is required to trap a 50 nm radius PS bead with an injected power of 10 mW [47]. Experimentally, 500 nm diameter PS beads have been trapped by injecting 6mW (at 1550nm) in a waveguide functionalized by a 20 gold NP chain, with a measured stiffness of -5.1 10^{-1} fN.nm^{-1} in the propagation direction (x). Considering the fibered optical injection losses in the waveguide, the stiffness is estimated at -10^{2} fN.nm^{-1}W^{-1}.

Chains of metallic nanostructures can be realized for any shape of resonant nanoparticles (disks, ellipsoidal cylinders, butterflies, ...), and thus adapted for different objects to be trapped, as represented in Figure 10 for a transverse dimer chain.

Besides, the spectral and spatial dependence of the MNP chains excitation allows realizing all-optical trapped object manipulation. Figure 11 shows the stable trapping positions (pale pink lines) versus the excitation wavelength in the case of a 4 MNP chain and 10mW injected power [48]. In this case, the integrated nanotweezers is designed to manipulate a biological object modelled as a spherical bead with a radius of 250 nm and with a refractive index as low as 1.38. By adjusting the source wavelength to regulate the phase mismatch of the supermodes housed by the structure, it is possible to manipulate the trapped object along the plasmonic chain. Other configurations of integrated plasmonic "conveyor belt" have been proposed, based on the MNP size diversity [49]. Such structures are also able to trap and self-assemble groups of nano-objects [50].

Preprints (www.preprints.org) | NOT PEER-REVIEWED | Posted: 17 October 2023 doi:10.20944/preprints202310.1041.v1

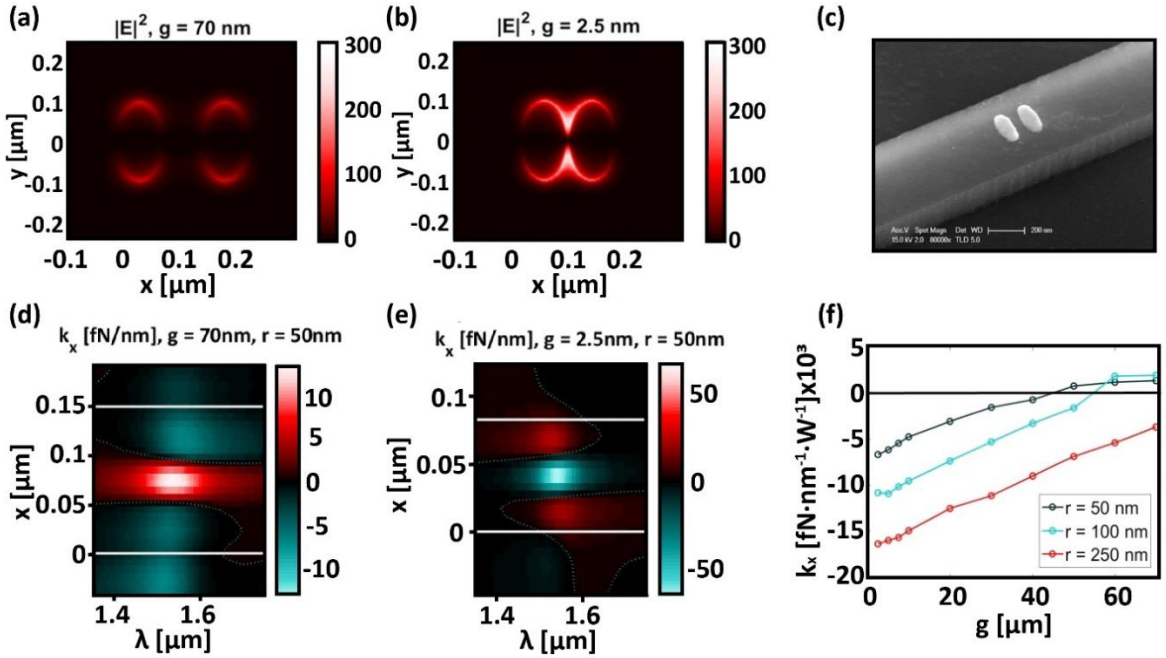

Figure 9. (**a**–**f**) Integrated longitudinal dimer chain for trapping nano-objects [47]. (**a**,**b**,**e**,**f**) FDTD simulation obtained for an injected power of 10 mW. (**a**,**b**) Squared absolute value of the electric field and (**d**,**e**) stiffness along the x-axis k_x calculated on the plane of the dimer top facet when the dimer gap g is equal to (**a**) 70 nm and (**b**) 2.5 nm, respectively. (**f**) Stiffness k_x as a function of the gap g calculated for different values of the radius of the bead interacting with the device. (**c**) Scanning electron microscope image of the fabricated sample.

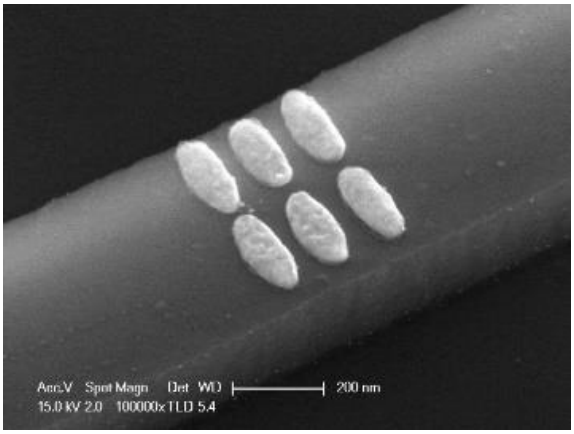

Figure 10. Scanning electron microscope image of a 3-periods dimer chain integrated on a SOI waveguide.

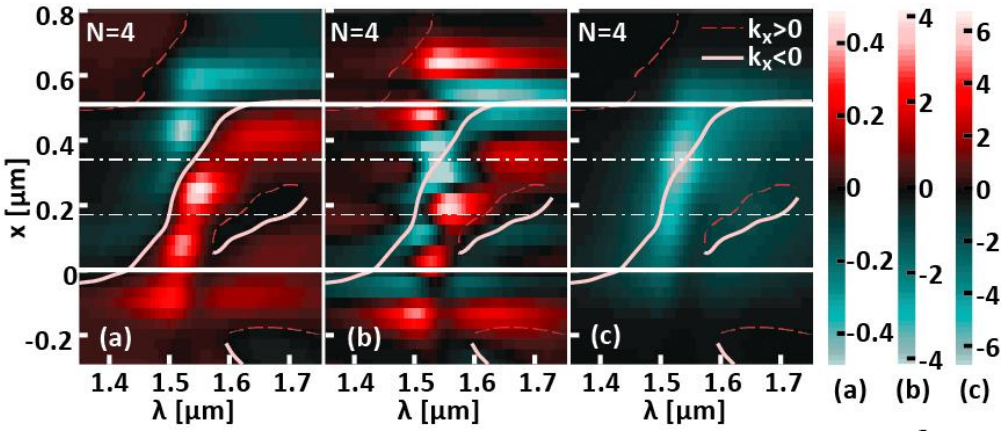

Preprints (www.preprints.org) | NOT PEER-REVIEWED | Posted: 17 October 2023 doi:10.20944/preprints202310.1041.v1

Figure 11. (**a**) Optical force [pN] and (**b**) stiffness [fN/nm] along the x-axis, as well as (**c**) optical force [pN] along the z-axis, calculated as a function of the wavelength and of the position of a spherical biological object. The latter is grazing along the x-axis on the top facet of a plasmonic chain composed of 4 NPs integrated on top of a SOI waveguide. The chain element spacing (centre to centre) is 150 nm. This device enables the trapping and displacement of the biological object along the plasmonic chain axis [48].

3.3. Plasmonic antennas

The integration of plasmonic antenna into photonic circuits allows wireless interconnection between adjacent circuits or their interfacing with a standard optical system. Various types of antennas, such as Vivaldi type antennas (leveraging propagative plasmons, [51–53]), Yagi-Uda antennas (acting as resonator-collector) or LSP chain antennas can be considered for this purpose. As previously discussed, the energy transfer between the PIC waveguide and the antenna is the key issue for the function efficiency.

In all these cases, it is imperative for the plasmonic structure to exhibit radiative behavior, meaning its dispersion curve must fall within the light cone, while also effectively coupling with the waveguide modes. In the case of Vivaldi antenna, these properties are obtained by changing progressively the antenna shape and the waveguide structure along the propagation. A progressive energy transfer is realized by evanescent coupling, and the excited plasmon radiates at the end of the suspended antenna. The integrated directivity is similar to the free space Vivaldi antenna and enables to target the receiver, itself integrated, as represented in Figure 12.

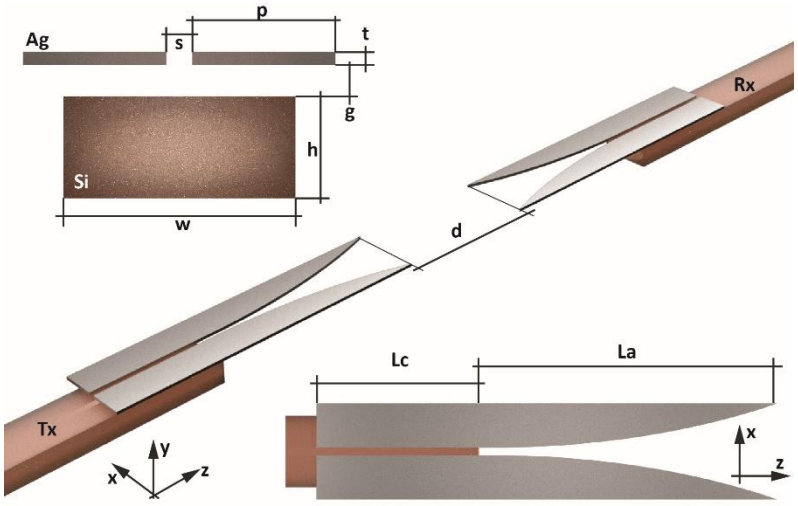

Figure 12. Vivaldi antenna integrated on a SOI waveguide as part of an on-chip optical interconnection system (inspired by [53]).

Integrated Yagi-Uda antenna is made of a resonant plasmonic "receiver", positioned between the "director" (made of several resonance-shifted resonators) and a "reflector" (wider metallic element). The radiative part of the antenna is the "receiver", whereas the other elements play roles of confinement (of incident signal) or directivity (of radiated signal) in the axe of the "director" chain. When the Yagi-Uda plasmonic antenna is integrated on a substrate or a waveguide, as represented in Figure 13, the emission is slightly deviated from the axis of the antenna elements in case of surrounding optical index asymmetry. The typical radiation diagram shows thus emission towards the higher index medium, usually the substrate. The angle depends mainly on the index contrast.

Preprints (www.preprints.org) | NOT PEER-REVIEWED | Posted: 17 October 2023 doi:10.20944/preprints202310.1041.v1

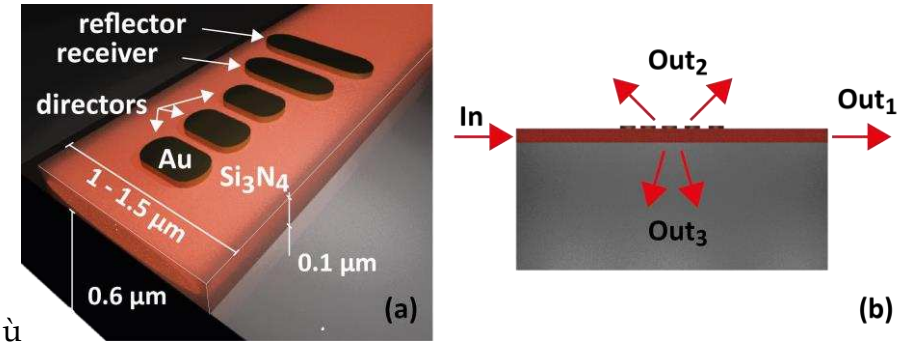

ù

Figure 13. Yagi-Uda antenna integrated in a waveguide. The radiation is preferentially directed towards the highest optical index (substrate). Inspired by [54].

Recently, it has been demonstrated that specific engineered arrangements of elementary nanoantennas, strategically positioned on the surface of a silicon waveguide, can couple the two orthogonal polarizations of incident light into different directions and modes of the underlying waveguide, thus achieving a demultiplexing function [55].

A periodic chain made of identical MNP can also realize controlled directivity "LSP" antenna, evanescently coupled to a dielectric waveguide. In order to obtain collective and radiative resonance, the chain is designed as a diffraction grating while keeping a sufficiently short period to enable dipole coupling along the chain [56,57]. The latter property enables efficient interfacing of the antenna with the dielectric waveguide (Figure 14). The diffraction grating controls the emission direction (period) and directivity (chain length). For symmetry reasons, as soon as the grating order is higher than 1 the light is diffracted simultaneously in two directions, toward the substrate and the superstrate. The emission angle is defined with respect to the guided propagation axis as follows, in the case of homogeneous surrounding index n_s: $\theta = arcsin\left(\frac{n_{eff}}{n_s} - \frac{m.\lambda}{d.n_s}\right)$ where d is the grating period, m the grating order and n_{eff} the effective index of the guided mode. With respect to usual dielectric or metallic gratings, this resonant chain grating offers additional degrees of freedom:

- The chain resonance modifies the coupling efficiency independently of the emission angle and directivity control: the MNP size is chosen to have resonant or resonant-shifted chain.
- The chain can be positioned freely around the waveguide, without diffraction efficiency modification as long as the chain and waveguide modes overlap remains similar.
- The chain period determines the emission angle, independently of the coupling efficiency.
- Several chains can be simultaneously excited, for example to shape the radiation diagram: two chains on both sides of the waveguide generate radiation similar to Young's slits interferences.

In Figure 14, such a double 8 ellipsoidal MNP chain with d=300nm is positioned at D=50nm from a silicon nitride waveguide. The minima of optical transmission through the waveguide indicate the chain resonances for three values of ellipses long axis radius a_y. The radiation diagrams are calculated for two different wavelengths: they show the independence of the emission angle and the coupling efficiency (proportional to the radiative power). This control of the coupling efficiency was verified experimentally [58]. It can vary from 10 to 50% by changing only the major axis of the nanocylinders a_y, offering control of the radiated power without changing the radiation diagram.

3.4. Integrated magnetoplasmonics

Plasmonics is particularly relevant for enhancing perturbative physical effects such as magneto-optics (MO) [59]. Magneto-optical effects are related to the action of the magnetization of a material on the propagation of an optical wave through it. This action is expressed by the non-diagonal elements of the permittivity tensor of the MO material, which is as follows, in the case of otherwise isotropic material:

Preprints (www.preprints.org) | NOT PEER-REVIEWED | Posted: 17 October 2023 doi:10.20944/preprints202310.1041.v1

$$\varepsilon = \begin{pmatrix} \varepsilon_{iso} & +ig_z & -ig_y \\ -ig_z & \varepsilon_{iso} & +ig_x \\ +ig_y & -ig_x & \varepsilon_{iso} \end{pmatrix} \quad (3)$$

where g_u (u=x,y,z) are the gyrotropy constants, which are complex values in the most general case. The interaction of an electromagnetic wave with a MO material impacts its electric field through the complex coupling of its components (E_x, E_y, E_z), which can modify the wave polarisation, amplitude and/or phase. Since the permittivity tensor is antisymmetric, this interaction is non-reciprocal: it is inversed by inversion of the propagation direction or the magnetisation direction. In other words, this effect induces time-symmetry breaking. Usual MO materials are either metallic (Fe, Co, Ni, and alloys), or dielectric like garnet oxides (BIG, YIG, Ce:YIG). Combined with a plasmonic metal, these materials induce magneto-plasmonic effects, with enhanced effective complex gyrotropies.

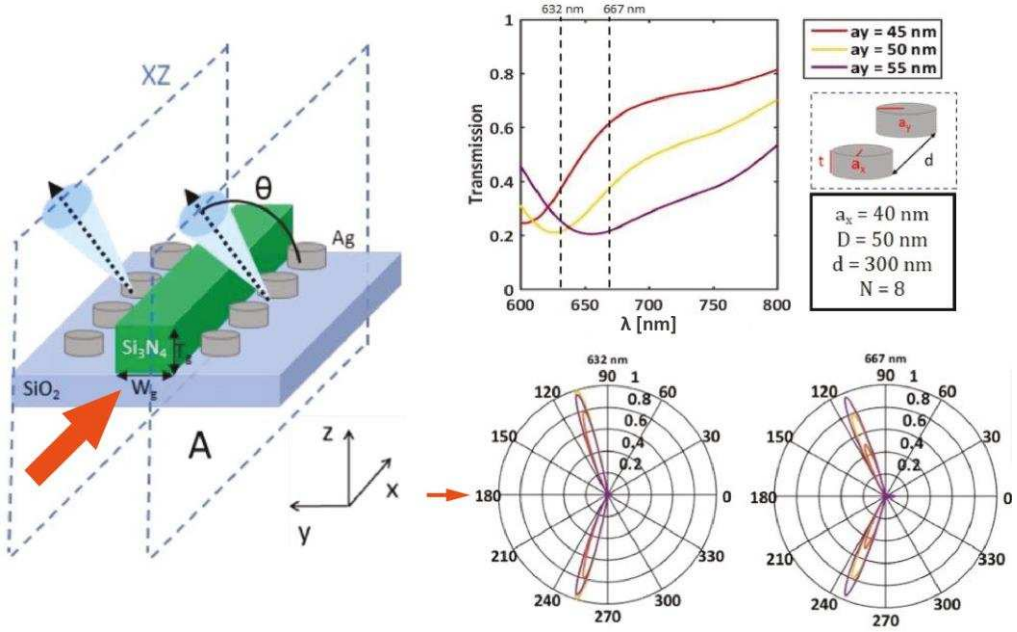

Figure 14. Array of integrated plasmonic nanoantennas dedicated to the independent control of directivity, direction and intensity of radiation, inspired by [58]. a_x and a_y represent the radii of the ellipsoidal sections of the NPs, t their thickness, N their number per chain, d their centre-to-centre distance, D their closest distance to the dielectric guide. The red arrow indicates the direction of light injection.

The main interest of these MO or magneto-plasmonic structures is to realize non-reciprocal transmission of the light, like optical isolation or circulation. The non-reciprocal transmission is obtained only if all the spatial symmetries are also broken, in addition to the time-symmetry breaking. The non-reciprocity of an integrated isolator is defined as the ratio between its forward and backward transmissions, denoted as T^+ et T^-, often expressed in decibel as $10\text{Log}(T^+/T^-)$. A figure of merit (FoM) Δ can be defined to account the trade-off between non-reciprocity and insertion losses:

$$\Delta = \begin{cases} \dfrac{T^+ - T^-}{T^+} & if \quad T^+ > T^- \\ \dfrac{T^+ - T^-}{T^-} & if \quad T^+ < T^- \end{cases} \quad (4)$$

Several MO effects have been identified, all related to the permittivity tensor and gyrotropies, but considering different configurations of light polarisation, magnetization orientations, and interaction nature (bulk or at interfaces) [60]. Among all these configurations, the most relevant for integrated guided structures is the TMOKE (Transverse Magneto-Optical Effect): indeed, TMOKE preserves the light polarisation, it only modifies the propagation wavevector of the light and it occurs at interfaces between MO and dielectric or metallic materials. Such a configuration is easily obtained

Preprints (www.preprints.org) | NOT PEER-REVIEWED | Posted: 17 October 2023 doi:10.20944/preprints202310.1041.v1

in multi-layered planar structures, and spatial symmetry breaking is also just a matter of appropriate geometry (Figure 15).

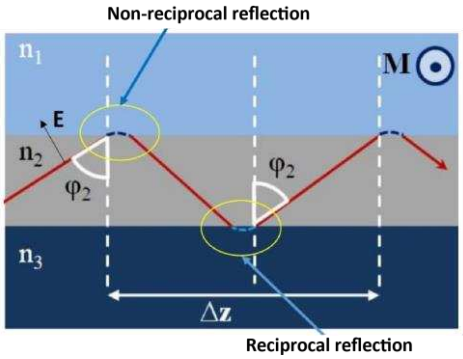

Figure 15. TMOKE (transverse magneto-optical Kerr effect) applied to a planar waveguide. The top layer (n_1) is a material with magneto-optical properties.

Many structures based on TMOKE have been demonstrated, based on: MO metallic layer deposited on dielectric or semiconductor waveguide, interacting with TE [61] or TM [62] mode; MO garnet transferred on a semiconductor interferometer [63] or on a ring resonator [64]; garnet interferometer including a thin silver film [65]; gold grating on alternating silver and garnet layers [66], gold grating on a garnet waveguide [67], In the latter structure, the non-reciprocal effect is enhanced by plasmonic light concentration, and in addition its sign is controlled by the grating slit modes coupling with the propagative surface plasmon. Such a way, non-reciprocity can be inversed by proper grating design, while keeping unchanged the magnetization direction.

Such a structure is represented in Figure 16: the gold grating is placed on the top of a MO garnet (BIG) waveguide, whose magnetization is in z direction. The guided TM mode is injected in the structure and interacts with the plasmonic top-grating and with the Fabry-Perot modes inside the grating slits. Their coupling induces anticrossing in the dispersion curves (Figure 16b) and non-reciprocity enhancement on each side of this anticrossing. Because of the resonant character of the structure the isolation is limited to a narrow bandwidth, and the FoM reaches 40%.

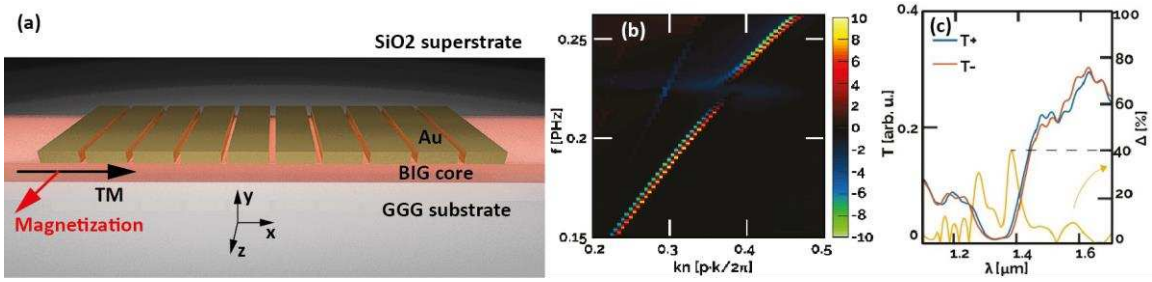

Figure 16. (**a**) Sketch of a non-reciprocal waveguide with integrated plasmonic grating on garnet. Here, the BIG layer is the magneto-optical material. (**b**) Non-reciprocal shift of the bandstructure and (**c**) non-reciprocal transmittances obtained by means of FDTD simulations [67].

Following the same principle, by positioning the plasmonic grating on the side of the waveguide, TE mode undergoes isolation ratio higher than 20dB (8 dB), with possible sign inversion and FoM above 1 (0.2) [68], with a gyrotropy of 0.1 (0.01).

More generally, in this kind of structure, plasmonics may also modify the global properties of the MO material: indeed, in the case of a purely real gyrotropy MO material, TMOKE only induces non-reciprocal phase shift on the propagating wave; thanks to the plasmonic interaction at the TMOKE interface, the global non-reciprocity also applies on the amplitude of the propagating wave [69].

Up to now the best experimentally demonstrated structures (using garnets) are nevertheless difficult to integrate in standard photonic circuits (Silicon or semiconductor) because of their crystallographic mismatch, despite promising results [70].

4. Conclusions

The integration of propagative or localized plasmonic structures on photonic waveguides brings a breakthrough toward the PICs miniaturisation, provided that their interfacing is efficient. Achieving high efficiency can be made possible through the engineering of guided mode coupling mechanisms. This engineering enables the utilization of plasmons within photonic circuits with moderation, offering an optimal balance between compactness, enhanced physical effects, and minimized losses. As shown here, numerous and diversified applications can be considered, especially thanks to the ease of technological processes. Indeed, nanofabrication of metallic structures is realized with standard process of photonics, without any additional complexity. Moreover, these structures are compatible with other planar systems like microfluidic systems for lab-on-chip (biosensors, optical tweezers, plasmonic manipulators, etc.), electronic systems for electron beam or X-rays sources, optoelectronic systems combining electrical injection, electrical generation of plasmons, or active photonic functions.

Author Contributions: Literature search, B.D.; Writing draft of manuscript, G.M. and B.D.; Revision and proof reading, B.D., V.Y. and G.M. All authors have read and agreed to the published version of the manuscript.

Institutional Review Board Statement: Not applicable.

Data Availability Statement: Not applicable.

Acknowledgments: The work presented in this article was partly supported by the RENATECH national network of technology centers, the French Defense Innovation Agency, and the PhOVéA OpenLab (CNRS-Stellantis). G.M is supported by a grant from Regione Puglia "Research for Innovation" (REFIN). REFIN is an intervention co-financed by the European Union under the POR Puglia 2014-2020, Priority Axis OT X "Investing in education, training and professional training for skills and lifelong learning" - Action 10.4 - DGR 1991/2018 - Notice 2/FSE/2020 n. 57 of 13/05/2019 (BURP n. 52 of 16/06/2019).

Conflicts of Interest: The authors declare no conflict of interest.

References

1. Lelit, M.; Słowikowski, M.; Filipiak, M.; Juchniewicz, M.; Stonio, B.; Michalak, B.; Pavłov, K.; Myśliwiec, M.; Wiśniewski, P.; Kaźmierczak, A.; et al. Passive Photonic Integrated Circuits Elements Fabricated on a Silicon Nitride Platform. *Materials (Basel)*. 2022, *15*.
2. Albiero, R.; Pentangelo, C.; Gardina, M.; Atzeni, S.; Ceccarelli, F.; Osellame, R. Toward Higher Integration Density in Femtosecond-Laser-Written Programmable Photonic Circuits. *Micromachines* 2022, *13*.
3. Korthorst, T.; Bogaerts, W.; Boning, D.; Heins, M.; Bergman, B. Photonic Integrated Circuit Design Methods and Tools. In *Integrated Photonics for Data Communication Applications*; Glick, M., Liao, L., Schmidtke, K.B.T.-I.P. for D.C.A., Eds.; Elsevier, 2023; pp. 335–367 ISBN 978-0-323-91224-2.
4. Maier, S. *Plasmonics: Fundamentals and Applications*; Springer, 2007; ISBN 0387331506.
5. Raether, H. *Surface Plasmons on Smooth and Rough Surfaces and on Gratings*; Springer-Verlag: Berlin, 1998;
6. Cheng, C.-W.; Gwo, S. Fundamentals of Plasmonic Materials. In *Plasmonic Materials and Metastructures*; Gwo, S., Alù, A., Li, X., Shih, C.-K.B.T.-P.M. and M., Eds.; Elsevier, 2024; pp. 3–33 ISBN 978-0-323-85379-8.
7. Sun, P.; Xu, P.; Zhu, K.; Zhou, Z. Silicon-Based Optoelectronics Enhanced by Hybrid Plasmon Polaritons: Bridging Dielectric Photonics and Nanoplasmonics. *Photonics* 2021, *8*.
8. Palik, E.D.; Ghosh, G. *Handbook of Optical Constants of Solids II*; Academic Press: Orlando, 1998; ISBN 0125444206 (alk. paper).
9. Bohren, C.F.; Huffman, D.R. *Absorption and Scattering of Light by Small Particles*; Wiley: New York, 1998;
10. Berini, P.; De Leon, I. Surface Plasmon-Polariton Amplifiers and Lasers. *Nat. Photonics* **2012**, *6*, 16–24, doi:10.1038/nphoton.2011.285.

11. Delacour, C.; Blaize, S.; Grosse, P.; Fedeli, J.M.; Bruyant, A.; Salas-Montiel, R.; Lerondel, G.; Chelnokov, A. Efficient Directional Coupling between Silicon and Copper Plasmonic Nanoslot Waveguides: Toward Metal-Oxide-Silicon Nanophotonics. *Nano Lett.* **2010**, *10*, 2922–2926, doi:10.1021/nl101065q.
12. Magno, G.; Grande, M.; Petruzzelli, V.; D'Orazio, A. High-Efficient Ultra-Short Vertical Long-Range Plasmonic Couplers. *J. Nanophotonics* **2012**, *6*, 061609, doi:10.1117/1.jnp.6.061609.
13. Magno, G.; Grande, M.; Petruzzelli, V.; D'Orazio, A. Numerical Analysis of the Coupling Mechanism in Long-Range Plasmonic Couplers at 155 Mm. *Opt. Lett.* **2013**, *38*, 46, doi:10.1364/ol.38.000046.
14. Tetienne, J.P.; Bousseksou, A.; Costantini, D.; De Wilde, Y.; Colombelli, R. Design of an Integrated Coupler for the Electrical Generation of Surface Plasmon Polaritons. *Opt. Express* **2011**, *19*, 18155–18163, doi:10.1364/OE.19.018155.
15. Kelly, K.L.; Coronado, E.; Zhao, L.L.; Schatz, G.C. The Optical Properties of Metal Nanoparticles: The Influence of Size, Shape, and Dielectric Environment. *ChemInform* **2003**, *34*, 668–677, doi:10.1002/chin.200316243.
16. Koenderink, A.F.; Polman, A. Complex Response and Polariton-like Dispersion Splitting in Periodic Metal Nanoparticle Chains. *Phys. Rev. B - Condens. Matter Mater. Phys.* **2006**, *74*, doi:10.1103/PhysRevB.74.033402.
17. Moritake, Y.; Ono, M.; Notomi, M. Far-Field Optical Imaging of Topological Edge States in Zigzag Plasmonic Chains. **2022**, *11*, 2183–2189, doi:doi:10.1515/nanoph-2021-0648.
18. Buendía, Á.; Sánchez-Gil, J.A.; Giannini, V. Exploiting Oriented Field Projectors to Open Topological Gaps in Plasmonic Nanoparticle Arrays. *ACS Photonics* **2023**, *10*, 464–474, doi:10.1021/acsphotonics.2c01526.
19. Yan, Q.; Cao, E.; Sun, Q.; Ao, Y.; Hu, X.; Shi, X.; Gong, Q.; Misawa, H. Near-Field Imaging and Time-Domain Dynamics of Photonic Topological Edge States in Plasmonic Nanochains. *Nano Lett.* **2021**, *21*, 9270–9278, doi:10.1021/acs.nanolett.1c03324.
20. He, Z.; Bobylev, D.A.; Smirnova, D.A.; Zhirihin, D. V; Gorlach, M.A.; Tuz, V.R. Reconfigurable Topological States in Arrays of Bianisotropic Particles. *ACS Photonics* **2022**, *9*, 2322–2326, doi:10.1021/acsphotonics.2c00309.
21. Sinev, I.S.; Mukhin, I.S.; Slobozhanyuk, A.P.; Poddubny, A.N.; Miroshnichenko, A.E.; Samusev, A.K.; Kivshar, Y.S. Mapping Plasmonic Topological States at the Nanoscale. *Nanoscale* **2015**, *7*, 11904–11908, doi:10.1039/C5NR00231A.
22. Gong, M.; Hu, P.; Song, Q.; Xiang, H.; Han, D. Bound States in the Continuum from a Symmetric Mode with a Dominant Toroidal Dipole Resonance. *Phys. Rev. A* **2022**, *105*, 33504, doi:10.1103/PhysRevA.105.033504.
23. Song, Q.; Yi, Z.; Xiang, H.; Han, D. Dynamics and Asymmetric Behavior of Loss-Induced Bound States in the Continuum in Momentum Space. *Phys. Rev. B* **2023**, *107*, 165142, doi:10.1103/PhysRevB.107.165142.
24. Jin, Y.; Wu, K.; Sheng, B.; Ma, W.; Chen, Z.; Li, X. Plasmonic Bound States in the Continuum to Tailor Exciton Emission of MoTe2. *Nanomaterials* 2023, *13*.
25. Magno, G.; Leroy, B.; Barat, D.; Pradere, L.; Dagens, B. Numerical Demonstration of Surface Lattice Resonance Excitation in Integrated Localized Surface Plasmon Waveguides. *Opt. Express* **2022**, *30*, 5835–5847, doi:10.1364/OE.449832.
26. Utyushev, A.D.; Zakomirnyi, V.I.; Rasskazov, I.L. Collective Lattice Resonances: Plasmonics and Beyond. *Rev. Phys.* **2021**, *6*, 100051, doi:https://doi.org/10.1016/j.revip.2021.100051.
27. Kravets, V.G.; Schedin, F.; Grigorenko, A.N. Extremely Narrow Plasmon Resonances Based on Diffraction Coupling of Localized Plasmons in Arrays of Metallic Nanoparticles. *Phys. Rev. Lett.* **2008**, *101*, 87403, doi:10.1103/PhysRevLett.101.087403.
28. Pikalov, A.M.; Dorofeenko, A. V; Lozovik, Y.E. Dispersion Relations for Plasmons in Complex-Shaped Nanoparticle Chains. *Phys. Rev. B* **2018**, *98*, 85134, doi:10.1103/PhysRevB.98.085134.
29. Chamanzar, M.; Xia, Z.; Yegnanarayanan, S.; Adibi, A. Hybrid Integrated Plasmonic-Photonic Waveguides for on-Chip Localized Surface Plasmon Resonance (LSPR) Sensing and Spectroscopy. *Opt. Express* **2013**, *21*, 32086, doi:10.1364/oe.21.032086.
30. Février, M.; Gogol, P.; Aassime, A.; Mégy, R.; Delacour, C.; Chelnokov, A.; Apuzzo, A.; Blaize, S.; Lourtioz, J.M.; Dagens, B. Giant Coupling Effect between Metal Nanoparticle Chain and Optical Waveguide. *Nano Lett.* **2012**, *12*, 1032–1037, doi:10.1021/nl204265f.
31. Novotny, L. Strong Coupling, Energy Splitting, and Level Crossings: A Classical Perspective. *Am. J. Phys.* **2010**, *78*, 1199–1202, doi:10.1119/1.3471177.

32. Magno, G.; Fevrier, M.; Gogol, P.; Aassime, A.; Bondi, A.; Mégy, R.; Dagens, B. Strong Coupling and Vortexes Assisted Slow Light in Plasmonic Chain-SOI Waveguide Systems. *Sci. Rep.* **2017**, *7*, doi:10.1038/s41598-017-07700-z.
33. Dagens, B.; Février, M.; Gogol, P.; Blaize, S.; Apuzzo, A.; Magno, G.; Mégy, R.; Lerondel, G. Direct Observation of Optical Field Phase Carving in the Vicinity of Plasmonic Metasurfaces. *Nano Lett.* **2016**, *16*, doi:10.1021/acs.nanolett.6b00435.
34. Li, Z.; Kim, M.-H.; Wang, C.; Han, Z.; Shrestha, S.; Overvig, A.C.; Lu, M.; Stein, A.; Agarwal, A.M.; Lončar, M.; et al. Controlling Propagation and Coupling of Waveguide Modes Using Phase-Gradient Metasurfaces. *Nat. Nanotechnol.* **2017**, *12*, 675–683, doi:10.1038/nnano.2017.50.
35. Divya, J.; Selvendran, S.; Raja, A.S.; Sivasubramanian, A. Surface Plasmon Based Plasmonic Sensors: A Review on Their Past, Present and Future. *Biosens. Bioelectron. X* **2022**, *11*, 100175, doi:https://doi.org/10.1016/j.biosx.2022.100175.
36. Shrivastav, A.M.; Cvelbar, U.; Abdulhalim, I. A Comprehensive Review on Plasmonic-Based Biosensors Used in Viral Diagnostics. *Commun. Biol.* **2021**, *4*, 70, doi:10.1038/s42003-020-01615-8.
37. Hamza, M.E.; Othman, M.A.; Swillam, M.A. Plasmonic Biosensors: Review. *Biology (Basel).* 2022, *11*.
38. Duan, Q.; Liu, Y.; Chang, S.; Chen, H.; Chen, J. Surface Plasmonic Sensors: Sensing Mechanism and Recent Applications. *Sensors* 2021, *21*.
39. Steglich, P.; Schasfoort, R.B.M. Surface Plasmon Resonance Imaging (SPRi) and Photonic Integrated Circuits (PIC) for COVID-19 Severity Monitoring. *COVID* 2022, *2*, 389–397.
40. Anker, J.N.; Hall, W.P.; Lyandres, O.; Shah, N.C.; Zhao, J.; Van Duyne, R.P. Biosensing with Plasmonic Nanosensors. *Nat. Mater.* **2008**, *7*, 442–453, doi:10.1038/nmat2162.
41. Kabashin, A. V.; Evans, P.; Pastkovsky, S.; Hendren, W.; Wurtz, G.A.; Atkinson, R.; Pollard, R.; Podolskiy, V.A.; Zayats, A. V. Plasmonic Nanorod Metamaterials for Biosensing. *Nat. Mater.* **2009**, *8*, 867–871, doi:10.1038/nmat2546.
42. Kretschmann, E.; Raether, H. Radiative Decay of Nonradiative Surface Plasmons Excited by Light. *Zeitschrift Für Naturforsch. Sect. A A J. Phys. Sci.* **1968**, *23*, 2135.
43. Février, M.; Gogol, P.; Barbillon, G.; Aassime, A.; Mégy, R.; Bartenlian, B.; Lourtioz, J.-M.; Dagens, B. Integration of Short Gold Nanoparticles Chain on SOI Waveguide toward Compact Integrated Bio-Sensors. *Opt. Express* **2012**, *20*, 17402, doi:10.1364/oe.20.017402.
44. Ashkin, A.; Dziedzic, J.M.; Bjorkholm, J.E.; Chu, S. Observation of a Single-Beam Gradient Force Optical Trap for Dielectric Particles. *Opt. Angular Momentum* **2016**, *11*, 196–198, doi:10.1364/ol.11.000288.
45. Falconi, M.C.; Magno, G.; Colosimo, S.; Yam, V.; Dagens, B.; Prudenzano, F. Design of a Half-Ring Plasmonic Tweezers for Environmental Monitoring. *Opt. Mater. X* **2022**, *13*, 100141, doi:https://doi.org/10.1016/j.omx.2022.100141.
46. Wong, H.M.K.; Righini, M.; Gates, J.C.; Smith, P.G.R.; Pruneri, V.; Quidant, R. On-a-Chip Surface Plasmon Tweezers. *Appl. Phys. Lett.* **2011**, *99*, 061107–061107, doi:10.1063/1.3625936.
47. Ecarnot, A.; Magno, G.; Yam, V.; Dagens, B. Ultra-Efficient Nanoparticle Trapping by Integrated Plasmonic Dimers. *Opt. Lett.* **2018**, *43*, 455, doi:10.1364/ol.43.000455.
48. Magno, G.; Ecarnot, A.; Pin, C.; Yam, V.; Gogol, P.; Mégy, R.; Cluzel, B.; Dagens, B. Integrated Plasmonic Nanotweezers for Nanoparticle Manipulation. *Opt. Lett.* **2016**, *41*, 3679, doi:10.1364/ol.41.003679.
49. Wang, G.; Ying, Z.; Ho, H.; Huang, Y.; Zou, N.; Zhang, X. Nano-Optical Conveyor Belt with Waveguide-Coupled Excitation. *Opt. Lett.* **2016**, *41*, 528, doi:10.1364/ol.41.000528.
50. Pin, C.; Magno, G.; Ecarnot, A.; Picard, E.; Hadji, E.; Yam, V.; de Fornel, F.; Dagens, B.; Cluzel, B. Seven at One Blow: Particle Cluster Stability in a Single Plasmonic Trap on a Silicon Waveguide. *ACS Photonics* **2020**, *7*, 1942–1949, doi:10.1021/acsphotonics.0c00637.
51. Calò, G.; Bellanca, G.; Alam, B.; Kaplan, A.E.; Bassi, P.; Petruzzelli, V. Array of Plasmonic Vivaldi Antennas Coupled to Silicon Waveguides for Wireless Networks through On-Chip Optical Technology - WiNOT. *Opt. Express* **2018**, *26*, 30267, doi:10.1364/oe.26.030267.
52. Fuschini, F.; Barbiroli, M.; Zoli, M.; Bellanca, G.; Calò, G.; Bassi, P.; Petruzzelli, V. Ray Tracing Modeling of Electromagnetic Propagation for On-Chip Wireless Optical Communications. *J. Low Power Electron. Appl.* **2018**, *8*, doi:10.3390/jlpea8040039.
53. Bellanca, G.; Calò, G.; Kaplan, A.E.; Bassi, P.; Petruzzelli, V. Integrated Vivaldi Plasmonic Antenna for Wireless On-Chip Optical Communications. *Opt. Express* **2017**, *25*, 16214, doi:10.1364/oe.25.016214.

54. Bernal Arango, F.; Kwadrin, A.; Koenderink, A.F. Plasmonic Antennas Hybridized with Dielectric Waveguides. *ACS Nano* **2012**, *6*, 10156–10167, doi:10.1021/nn303907r.
55. Guo, R.; Decker, M.; Setzpfandt, F.; Gai, X.; Choi, D.-Y.; Kiselev, R.; Chipouline, A.; Staude, I.; Pertsch, T.; Neshev, D.N.; et al. High–Bit Rate Ultra-Compact Light Routing with Mode-Selective on-Chip Nanoantennas. *Sci. Adv.* **2023**, *3*, e1700007, doi:10.1126/sciadv.1700007.
56. Fevrier, M.; Gogol, P.; Aassime, A.; Megy, R.; Bouville, D.; Lourtioz, J.M.; Dagens, B. Localized Surface Plasmon Bragg Grating on SOI Waveguide at Telecom Wavelengths. *Appl. Phys. A Mater. Sci. Process.* **2012**, *109*, 935–942, doi:10.1007/s00339-012-7395-3.
57. Février, M.; Gogol, P.; Lourtioz, J.-M.; Dagens, B. Metallic Nanoparticle Chains on Dielectric Waveguides: Coupled and Uncoupled Situations Compared. *Opt. Express* **2013**, *21*, 24504, doi:10.1364/oe.21.024504.
58. Leroy, B.; Magno, G.; Barat, D.; Pradere, L.; Dagens, B. Integrated Nanoantenna Gratings for Planar Holographic Signalisation System. In Proceedings of the Asia Communications and Photonics Conference, ACP; 2018; Vol. 2018-Octob.
59. Maccaferri, N.; Gabbani, A.; Pineider, F.; Kaihara, T.; Tapani, T.; Vavassori, P. Magnetoplasmonics in Confined Geometries: Current Challenges and Future Opportunities. *Appl. Phys. Lett.* **2023**, *122*, 120502, doi:10.1063/5.0136941.
60. Zvezdin, A.K.; Kotov, V.A. Modern Magnetooptics and Magnetooptical Materials. *Mod. Magnetooptics Magnetooptical Mater.* **1997**, doi:10.1887/075030362x.
61. Shimizu, H.; Nakano, Y. Fabrication and Characterization of an InGaAsp/InP Active Waveguide Optical Isolator with 14.7 DB/Mm TE Mode Nonreciprocal Attenuation. *J. Light. Technol.* **2006**, *24*, 38–43, doi:10.1109/JLT.2005.861135.
62. Van Parys, W.; Moeyersoon, B.; Van Thourhout, D.; Baets, R.; Vanwolleghem, M.; Dagens, B.; Decobert, J.; Le Gouezigou, O.; Make, D.; Vanheertum, R.; et al. Transverse Magnetic Mode Nonreciprocal Propagation in an Amplifying AlGaInAs/InP Optical Waveguide Isolator. *Appl. Phys. Lett.* **2006**, *88*, 71115, doi:10.1063/1.2174106.
63. Yokoi, H.; Mizumoto, T.; Shoji, Y. Optical Nonreciprocal Devices with a Silicon Guiding Layer Fabricated by Wafer Bonding. *Appl. Opt.* **2003**, *42*, 6605, doi:10.1364/ao.42.006605.
64. Tien, M.-C.; Mizumoto, T.; Pintus, P.; Kromer, H.; Bowers, J.E. Silicon Ring Isolators with Bonded Nonreciprocal Magneto-Optic Garnets. *Opt. Express* **2011**, *19*, 11740, doi:10.1364/oe.19.011740.
65. Firby, C.J.; Elezzabi, A.Y. Magnetoplasmonic Isolators Utilizing the Nonreciprocal Phase Shift. *Opt. Lett.* **2016**, *41*, 563, doi:10.1364/ol.41.000563.
66. Díaz-Valencia, B.F.; Porras-Montenegro, N.; Oliveira, O.N.J.; Mejía-Salazar, J.R. Nanostructured Hyperbolic Metamaterials for Magnetoplasmonic Sensors. *ACS Appl. Nano Mater.* **2022**, *5*, 1740–1744, doi:10.1021/acsanm.1c04310.
67. Magno, G.; Yam, V.; Dagens, B. Integrated Magneto-Plasmonics for Non-Reciprocal Optical Devices. In Proceedings of the ECIO, Session M2: Advanced Materials; Eindhoven, Nederlands, 2017.
68. Abadian, S.; Magno, G.; Yam, V.; Dagens, B. Integrated Magneto-Plasmonic Isolation Enhancement Based on Coupled Resonances in Subwavelength Gold Grating. *Opt. Commun.* **2021**, *483*, 126633, doi:https://doi.org/10.1016/j.optcom.2020.126633.
69. Belotelov, V.I.; Akimov, I.A.; Pohl, M.; Kotov, V.A.; Kasture, S.; Vengurlekar, A.S.; Gopal, A.V.; Yakovlev, D.R.; Zvezdin, A.K.; Bayer, M. Enhanced Magneto-Optical Effects in Magnetoplasmonic Crystals. *Nat. Nanotechnol.* **2011**, *6*, 370–376, doi:10.1038/nnano.2011.54.
70. Yan, W.; Yang, Y.; Liu, S.; Zhang, Y.; Xia, S.; Kang, T.; Yang, W.; Qin, J.; Deng, L.; Bi, L. Waveguide-Integrated High-Performance Magneto-Optical Isolators and Circulators on Silicon Nitride Platforms. *Optica* **2020**, *7*, 1555, doi:10.1364/optica.408458.